ACS OMEGA

Open Access

http://pubs.acs.org/journal/acsodf

Article

Isolation, Characterization, In Vitro and In Silico Assessment of Undescribed Bioactive Constituents from *Pterocarpus santalinus* L. Heartwood

Priya Darshani, Shreya Sen Sarma, Rahul L. Gajbhiye, Amit K. Srivastava, and Deepak Kumar*

Cite This: *ACS Omega* 2024, 9, 49013−49022

Read Online

ACCESS | Metrics & More | Article Recommendations | Supporting Information

ABSTRACT: *Pterocarpus santalinus* heartwood is well acknowledged for its medicinal properties and use in the furniture and handicraft industries. Owing to its medicinal properties, the present investigation aims to isolate and characterize the secondary metabolites from the heartwood. The investigation led to the isolation of one undescribed dehydropterocarpan and eleven known compounds. *P. santalinus*heartwood is found to be a new source for six compounds. Interestingly, the undescribed dehydropterocarpan is transformed into an artifact, which led us to understand the biosynthetic correlations. The isolated compounds displayed moderate inhibition of α-glucosidase and α-amylase. The enzymatic assay outcome is further complimented with the in silico docking analysis. We have also evaluated the compounds for their drug-likeness properties, which align with the desired characteristics of potential drug candidates.

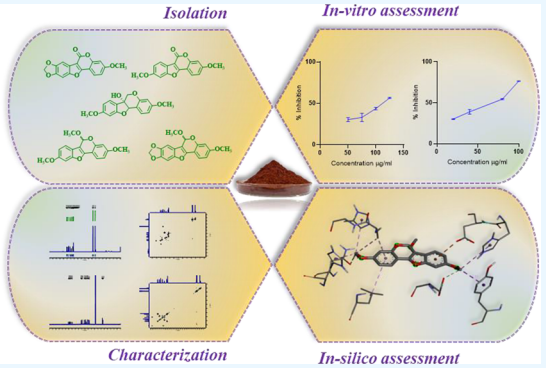

1. INTRODUCTION

Pterocarpus santalinus L. (PS; family: Fabaceae) is generally known as red sanders, red sandalwood, and rakt-chandan. Its natural habitat is restricted to the forest range located in the Andhra Pradesh region of Southern India. The elegant, deep red colored heartwood is one of the distinguished characteristics of the plant and thus commercially exploited for making furniture, musical instruments, and handicrafts.[1−3] Along with its significant commercial value, *P. santalinus* heartwood bears tremendous medicinal properties. The heartwood of the plant has been extensively studied for its anti-inflammatory,[4] antiviral,[5] cytotoxic,[4] antioxidant,[6] monoamine oxidase inhibition,[7] and antidiabetic activities.[8]

In the traditional system of medicine, PS has been described for its beneficial properties against fever, bronchitis, ulcers, and blood glucose-lowering properties.[1,8] These massive pharmacological properties of the plant are related to the abundance of different classes of phytochemicals. Previous phytochemical investigations on *P. santalinus* heartwood confirmed the occurrence of sesquiterpenoids, flavonoids, isoflavonoids, lignans, pterocarpans, coumarins, aurons, chalcones, pigments, stilbenes, and phenolic compounds.[1,3−5,9−12] Most of the antidiabetic activity of *P. santalinus* has been carried out on whole extract, and the chemical component responsible for the activity remains unexplored.[8,13]

Therefore, the present investigation aims to isolate and characterize constituents from the heartwood and further explore their α-glucosidase and α-amylase inhibitory potential. α-Glucosidase inhibitors have proven their utility as clinically approved drugs for managing postprandial hyperglycemia, a matter of concern for patients with diabetes mellitus. Postprandial hyperglycemia is characterized by the sudden rise in the blood glucose level after meals; therefore, α-glucosidase inhibitors are used to inhibit the enzyme responsible for releasing absorbable monosaccharides. It is pertinent to mention that α-amylase cleaves the polysaccharides into disaccharides, which release the monosaccharides on the action of α-glucosidase.[14,15]

The phytochemical investigation of PS heartwood led to the isolation of one undescribed pterocarpene and eleven known compounds. Of these, six compounds are being reported for the first time from *P. santalinus* heartwood and two as natural products. Further, in silico molecular docking analysis and Swiss-ADME studies were carried out on all the compounds to investigate the drug-likeness.

2. RESULTS AND DISCUSSION

2.1. Isolation and Characterization of Undescribed Constituents. The isolation of compounds (Figure 1) was achieved by subfractionation followed by purification of PSTF

Received: December 19, 2023
Revised: March 20, 2024
Accepted: March 28, 2024
Published: December 2, 2024

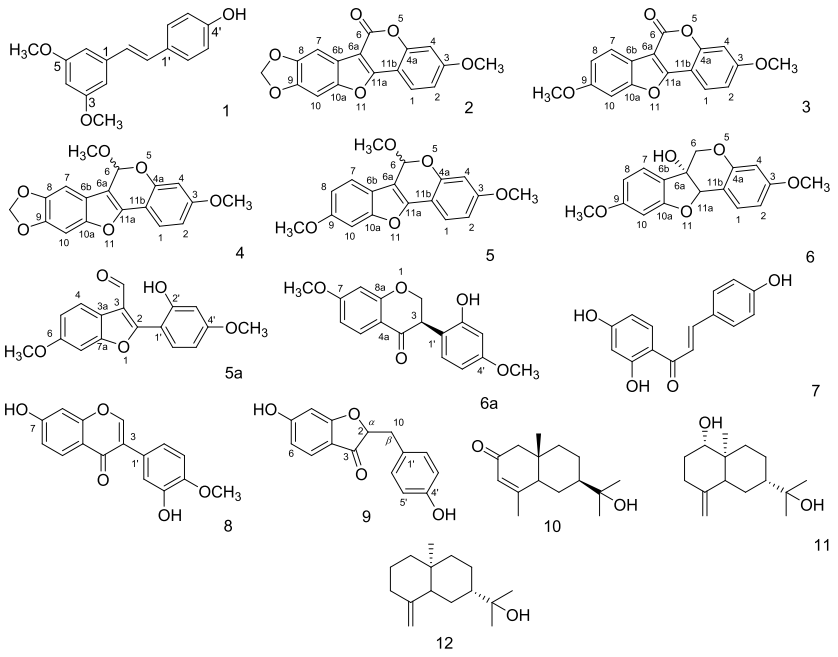

Figure 1. Structures of compounds **1**−**12**, **5a**, and **6a**.

Table 1. ^{1}H and ^{13}C Spectroscopic Data of Compounds 2−6

position	2		3		4		5		6	
	δ_H	δ_c	δ_H	δ_c	δ_H	δ_c	δ_H	δ_c	δ_H	δ_c
1	7.85 (1H, *d*, *J* = 8.4 Hz)	122.44	7.86 (1H, *d*, *J* = 8.4 Hz)	122.59	7.52 (1H, *d*, *J* = 8.4 Hz)	121.47	7.56 (1H, *d*, *J* = 8.4 Hz)	121.60	7.35 (1H, *d*, *J* = 9 Hz)	131.92
2	6.97 (1H, *dd*, *J* = 1.8, 8.4 Hz)	113.18	6.96 (1H, *dd*, *J* = 2.4, 9.0 Hz)	113.17	6.64 (1H, *dd*, *J* = 2.4, 8.4 Hz)	108.33	6.66 (1H, *dd*, *J* = 2.4, 8.4 Hz)	108.28	6.63 (1H, *dd*, *J* = 2.4, 8.4 Hz)	109.76
3		162.62		162.73		161.08		161.14		160.97
4	6.98 (1H, *brs*)	101.61	6.97 (1H, *brs*)	101.57	6.67 (1H, *d*, *J* = 2.4 Hz)	102.50	6.70 (1H, *d*, *J* = 2.4 Hz)	102.48	6.41 (1H, *d*, *J* = 2.4 Hz)	101.62
4a		155.00		155.26		153.29		153.45		155.74
6		158.63		158.64	6.56 (1H, *s*)	98.52	6.62 (1H, *s*)	98.62	4.15 (1H, *d*, 11.4 Hz) 3.98 (1H, d, 11.4 Hz)	69.65
6a		117.25		116.79		119.08		119.12		76.58
6b		104.18		103.66		106.55		105.89		120.23
7	7.47 (1H, *s*)	100.34	7.94 (1H, *d*, *J* = 9 Hz)	121.76	7.04 (1H, *s*)	94.23	7.39 (1H, *d*, *J* = 8.4 Hz)	118.88	7.19 (1H, *d*, *J* = 8.4 Hz)	123.94
8		146.28	7.04 (1H, *dd*, *J* = 8.4, 2.4 Hz)	113.33		145.11	6.92 (1H, *dd*, *J* = 2.4, 8.4 Hz)	112.15	6.48 (1H, *dd*, *J* = 1.8, 8.4 Hz)	107.67
9		147.54		159.39		146.02		158.06		162.38
10	7.12 (1H, *s*)	94.16	7.15 (1H, *d*, *J* = 2.4 Hz)	96.98	6.89 (1H, *s*)	97.69	7.11 (1H, *d*, *J* = 1.8 Hz)	96.81	6.36 (1H, *d*, *J* = 2.4 Hz)	97.04
10a		150.72		156.60		150.45		156.34		160.77
11a		160.15		160.22		149.57		149.24	5.23 (1H, *s*)	84.88
11b		106.36		106.28		110.13		108.32		112.48
9-*O*-CH_3			3.90 (3H, *s*)	55.97			3.88 (3H, *s*)	55.94	3.72 (3H, *s*)	55.39
6-*O*-CH_3					3.54 (3H, *s*)	54.53	3.56 (3H, *s*)	54.49		
3-*O*-CH_3	3.91 (3H, *s*)	55.98	3.91 (3H, *s*)	56.01	3.84 (3H, *s*)	55.63	3.86 (3H, *s*)	55.63	3.74 (3H, *s*)	55.53
-*O*-CH_2-*O*-	6.08 (2H, *s*)	102.12			5.99 (1H, *d*, *J* = 1.2 Hz)	101.59				
					6.00 (1H, *d*, *J* = 1.2 Hz)					

$CDCl_3$; ^{1}H NMR: 600 MHz; ^{13}C NMR: 150 MHz

(toluene fraction) and PSEAF (ethyl acetate fraction), and characterized by the combined use of mass, IR, ^{1}H, ^{13}C, and 2D NMR. The NMR spectroscopic data of compounds **2**−**6**, **8**−**9**, **5a**, and **6a** are detailed in Tables 1−3.

Compound **5** was obtained as a white amorphous solid, which gave a pseudomolecular ion peak in the ESI-HR-MS spectrum at *m*/*z* 313.1075 $[M + H]^+$ (calculated for $C_{18}H_{17}O_5$, 313.1076) corresponding to molecular formula $C_{18}H_{16}O_5$, indicating the presence of 11 degrees of unsaturation. The intense fluorescence on UV irradiation on TLC analysis, UV absorption maxima at 209, 325, and 337 nm, and IR bands corresponding to the aromatic ring (1647, 1613, 1500 cm^{-1})

https://doi.org/10.1021/acsomega.3c10180
ACS Omega 2024, 9, 49013−49022

Table 2. ^{1}H and ^{13}C Spectroscopic Data of Compounds 8, 6a

position	8		6a	
	δ_H	δ_c	δ_H	δ_c
2	8.12 (1H, *s*)	154.80	4.96 (1H, *dd*, *J* = 4.8, 12 Hz)	70.09
			4.82 (1H, *dd*, *J* = 4.8, 12 Hz)	
3		125.91	3.92 (1H, *m*)	45.61
4		178.15		193.06
4a		116.31		112.74
5	8.03 (1H, *d*, *J* = 8.4 Hz)	128.44	7.84 (1H, *d*, *J* = 9 Hz),	130.09
6	6.97 (1H, *brs*)	116.84	6.58 (1H, *d*, *J* = 2.4, 9 Hz)	110.14
7		165.43		167.20
8	6.82 (1H, *d*, *J* = 1.2 Hz)	103.31	6.44 (1H, *d*, *J* = 1.8 Hz)	100.72
8a		159.88		163.95
1′		124.87		115.21
2′	7.03 (1H, *brs*)	114.12		156.84
3′		148.78	6.54 (1H, *d*, *J* = 2.4 Hz)	103.58
4′		147.83		160.87
5′	6.97 (1H, *brs*)	116.18	6.46 (1H, *d*, *J* = 1.8, 9.0 Hz)	107.32
6′	6.92 (1H, *dd*, *J* = 9.0, 2.4 Hz)	122.89	7.42 (1H, *d*, *J* = 8.4 Hz)	127.44
4′-*O*-CH_3	3.87 (3H, *s*)	56.44	3.85 (3H, *s*)	55.91
−OH			8.39 (1H, *s*)	
7-*O*-CH_3			3.75 (3H, *s*)	55.46
	MeOD; ^{1}H NMR: 400 MHz; ^{13}C NMR: 100 MHz		$CDCl_3$; ^{1}H NMR: 600 MHz; ^{13}C NMR: 150 MHz	

Table 3. ^{1}H and ^{13}C Spectroscopic Data of Compounds 9, 5a

position	9		5a	
	δ_H	δ_c	δ_H	δ_c
2	5.39 (1H, *dd*, *J* = 2.8, 12.8 Hz)	81.03		162.39
3		193.55		118.54
3a				117.22
4		114.88	8.07 (1H, *d*, *J* = 8.4 Hz)	122.38
5	7.73 (1H, *d*, *J* = 8.8 Hz)	129.84	7.01 (1H, *dd*, *J* = 1.8, 9.0 Hz)	113.68
6	6.50 (1H, *dd*, *J* = 2.4, 8.8 Hz)	111.86		159.16
7		165.59	7.07 (1H, *d*, *J* = 1.8 Hz)	96.01
7a				154.84
8	6.36 (1H, *d*, *J* = 2.4 Hz)	103.85		
9		167.06		
10	3.06 (1H, *dd*, *J* = 13.2, 17.2 Hz)	44.94		
	2.70 (1H, *dd*, *J* = 3.2, 17.2 Hz)			
1′		131.37		108.42
2′	7.33 (1H, *d*, *J* = 8.8 Hz)	129.01		156.76
3′	6.83 (1H, *d*, *J* = 8.4 Hz)	116.31	6.64 (1H, *d*, *J* = 1.8 Hz)	103.06
4′		158.96		163.76
5′	6.83 (1H, *d*, *J* = 8.4 Hz)	116.31	6.66 (1H, *dd*, *J* = 1.8, 9.0 Hz)	108.42
6′	7.33 (1H, *d*, *J* = 8.8 Hz)	129.01	7.50 (1H, *d*, *J* = 8.4 Hz)	132.43
4′-*O*-CH_3			3.88 (3H, *s*)	55.74
−CHO			10.17 (1H, s)	187.40
6-*O*-CH_3			3.88 (3H, *s*)	55.97
	MeOD; ^{1}H NMR: 400 MHz; ^{13}C NMR: 100 MHz		$CDCl_3$; ^{1}H NMR: 600 MHz; ^{13}C NMR: 150 MHz	

and aromatic C−O (1226, 1025 cm^{-1}) collectively indicated the presence of pterocarpene moiety in concurrence with ^{1}H and ^{13}C spectroscopic data.[16,17]

It displayed eighteen carbon signals in its ^{13}C NMR spectrum, including three *O*-methyl carbon signals at δ_c 54.49, 55.63, and 55.94. The remaining fifteen carbon signals appeared in the aromatic range, including five oxygenated aromatic carbon signals at δ_c 149.24−161.14. The multiplicity of the individual resonance determined using DEPT revealed the presence of seven methines, three methyl, and eight quaternary resonances. In support, the ^{1}H NMR spectrum of compound **5** displayed six aromatic signals and a singlet at δ_H 6.62. The aromatic protons at δ_H 7.56 (1H, *d*, *J* = 8.4 Hz, H-1), 6.70 (1H, *d*, *J* = 2.4, H-4), 6.66 (1H, *dd*, *J* = 2.4, 8.4 Hz, H-2) and 7.39 (1H, *d*, *J* = 8.4 Hz, H-7), 7.11 (1H, *d*, *J* = 1.8 Hz, H-10), 6.92 (1H, *dd*, *J* = 2.4, 8.4 Hz, H-8) revealed two sets of typical ABX pattern.

The assignments for the ABX-1 system were ascertained from the ^{1}H-^{1}H COSY δ_H/δ_H 7.56/6.66, HSQC δ_c/δ_H 121.60/7.56, 108.28/6.66, 102.48/6.70 and HMBC δ_c/δ_H 121.60/6.66, 108.28/7.56, 102.48/6.66, 108.28/6.70 correlations. Similarly, the assignments for the ABX-2 system were

https://doi.org/10.1021/acsomega.3c10180
ACS Omega 2024, 9, 49013−49022

ascertained from the ^{1}H-^{1}H COSY δ_H/δ_H 7.39/6.92, HSQC δ_c/δ_H 118.88/7.39, 112.15/6.92, 96.81/7.11 and HMBC δ_c/δ_H 112.15/7.39, 118.88/6.92, 112.15/7.11, 96.81/6.92 correlations. The signals at δ_H 3.56 (3H, *s*), 3.86 (3H, *s*), and 3.88 (3H, *s*) were assigned to three *O*-methyl groups; of these the signal arising at δ_c/δ_H 55.63/3.86 was assigned to ABX-1 ring system owing to the HMBC cross peaks between $\delta_H/\delta_c/\delta_H$ 7.56/161.14/3.86 and δ_c/δ_H 55.63/3.88 was assigned to ABX-2 system following the HMBC cross peaks between $\delta_H/\delta_c/\delta_H$ 7.39/158.06/3.88 (Figure 2).

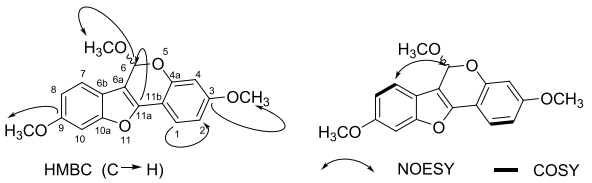

Figure 2. Selected HMBC, ^{1}H-^{1}H COSY, and NOESY correlations of **5**.

A careful examination of the NMR spectra revealed a close resemblance to that of anhydrovariabilin (3,9-dimethoxypterocarpene) except for an additional *O*-methyl group at C-6 position. Thus, compound **5** was identified as 6-*O*-methyl anhydrovariabilin, a pterocarpene {6H-benzofuro [3,2-c][1] benzopyran or 6a,11a-dehydropterocarpan} class of molecule which are relatively less common in nature.[18,19] The attachment of the *O*-methyl group at C-6 was ascertained by the HSQC correlation between δ_c/δ_H 98.62/6.62 (C-6), δ_c/δ_H 54.49/3.56 (-*O*-CH_3), and HMBC cross peaks between δ_c/δ_H 98.62/3.56 and 54.49/6.62. The assignments of the heterocyclic rings were deduced by extending the HMBC correlations δ_c/δ_H 153.45/6.62 (C-4a), 119.12/6.62 (C-6a), 149.24/6.62 (C-11a), 108.32/6.62 (C-6b). The NOESY correlations δ_H/δ_H 7.39/6.62 (CH-7/CH-6) allowed the confirmation of the pterocarpene skeleton.[16,17] Hence, compound **5** was characterized as 3,6,9-trimethoxy-6H-benzofuro [3,2-c][1] benzopyran (6-*O*-methyl anhydrovariabilin or 3,6,9-trimethoxypterocarpene) (Figures S1−S12).

Compound **4** was obtained as a white amorphous solid, which gave a pseudomolecular ion peak in the ESI-HR-MS +ve spectrum at *m*/*z* 327.0855 $[M + H]^+$ (calculated for $C_{18}H_{15}O_6$, 327.0869). It also indicated the presence of pterocarpene moiety in concurrence with ^{1}H and ^{13}C spectroscopic data.[16,17] It displayed similarity with compound **5** except for a methylenedioxy group instead of a methoxy. The attachment of methylenedioxy group (δ_c/δ_H 101.59/5.99−6.00) at C8 = C9 was deduced from the HMBC correlation (δ_c/δ_H 145.11/5.99−6.00, 146.02/5.99−6.00). Accordingly, compound **4** was characterized as 3,6-dimethoxy-8,9-methylenedioxy-6H-benzofuro-[3,2-C][1]benzopyran (3,6-dimethoxy-8,9-methylenedioxy pterocarpene). It is being reported for the first time as a natural compound from *P. santalinus* heartwood, along with the detailed assignments of the NMR data.[20]

Compound **2**, white crystalline solid, {ESI-HR-MS *m*/*z* 311.0577 $[M + H]^+$ (calculated for $C_{17}H_{11}O_6$, 311.0556} indicated 13 degrees of unsaturation owing to the molecular formula $C_{17}H_{10}O_6$. It displayed an intense blue fluorescence on UV irradiation on TLC, and PDA analysis showed UV absorption maxima at 210, 243, and 347 nm. It displayed a characteristic IR absorption band at 1738 cm^{-1} corresponding to *α*,*β* unsaturated *δ* lactone. These pieces of evidence collectively indicated the presence of the coumestane skeleton.[21−23] This observation is further supported by a distinct downfield shifted signal at δ_c 160.15 due to the synergistic effect of electron deficiency at *β*-position to the *α*,*β*-unsaturated lactone, and electron-withdrawing effect of furan moiety of coumestane.[21,23] The presence of methylenedioxy group (δ_c/δ_H 102.12/6.08) at C8 = C9 was confirmed from the HMBC correlation between δ_c/δ_H 146.28/6.08 and 147.54/6.08. Thus, compound **2** was characterized as 3-methoxy-8,9-methylenedioxycoumestan (medicagol methyl ether or flemichapparin C). The compound has been reported for the first time from *P. santalinus* heartwood, and ambiguity in the assignments of the spectroscopic data has been corrected by the extensive use of 1D and 2D NMR spectroscopy.[23,24]

Compound **3** was obtained as a white solid, which gave a pseudomolecular ion peak in the ESI-HR-MS at *m*/*z* 297.0560 $[M + H]^+$ (calculated for $C_{17}H_{13}O_5$, 297.0763) corresponding to molecular formula $C_{17}H_{12}O_5$ indicating 12 degrees of unsaturation and displayed the presence of coumestane skeleton.[21,23] Compound **3** was characterized as 3,9-dimethoxy-6H-benzofuro-[3,2-C] chromen-6-one, a derivative of compound **2** having 3,9-dimethoxy instead of 3-methoxy-8,9-methylenedioxy moieties. The compound has previously been reported synthetically, and *P. santalinus* heartwood appears to be the only natural source. Its spectroscopic data are consistent with those reported earlier; however, the assignments are achieved for the first time by extensive use of 1D and 2D NMR spectroscopy.[25,26]

Compound **6** was obtained as a yellow solid, which gave a pseudomolecular ion peak in the ESI-HR-MS +ve spectrum at *m*/*z* 301.1067 (calculated for $C_{17}H_{17}O_5$, 301.1076), which indicated the presence of 10 degrees of unsaturation ($C_{17}H_{16}O_5$). A careful examination of its spectroscopic data in comparison with compound **3** revealed shifting of C-6 from δ_c 158.64 (C═O) to δ_c 69.65 (CH_2) along with significant changes in the chemical shifts corresponding to heterocyclic ring. Detailed investigation in concurrence with the weak NOESY correlations δ_H/δ_H 7.19/3.98 (CH-7/CH_2-6) and 5.23/7.35 (CH-11a/CH-1) allowed the confirmation of 6a-hydroxypterocarpan skeleton.[16,17] Accordingly, compound **6** was characterized as 6a,11a-dihydro-3,9-dimethoxy-6H-benzofuro[3,2-c]chromen-6a-ol (variabilin). It is being reported for the first time from *P. santalinus* heartwood, and its spectroscopic data were found to be consistent with those reported earlier.[27,28]

Compound **9** was obtained as a light yellow solid, which gave a pseudomolecular ion in its ESI-HR-MS spectrum at *m*/*z* 257.0807 $[M + H]^+$ (calculated for $C_{15}H_{13}O_4$, 257.0814) corresponding to molecular formula $C_{15}H_{12}O_4$ and 10 degrees of unsaturation. The intense fluorescence on UV irradiation on TLC analysis, UV absorption maxima at 214, 274, and 306 nm, and IR bands corresponding to cyclic ketone (1593 cm^{-1}), hydroxy (3235 cm^{-1}), aromatic functionalities collectively indicated the presence of aurone type moiety in concurrence with ^{1}H and ^{13}C spectroscopic data.[29−31] The spectroscopic data revealed the presence of tri- and disubstituted aromatic rings; in addition, the signals corresponding to the methylene group at δ_C/δ_H 44.94/3.06−2.70 and oxygenated downfield signal at δ_C/δ_H 81.03/5.39 indicated the presence methylene linkage and thus confirmed the presence of dihydro-aurone skeleton bearing hydroxyl group on each of the aromatic ring.[29−31] A careful examination of the NMR spectra reveals a close resemblance with hispidol. The compound was

https://doi.org/10.1021/acsomega.3c10180
ACS Omega 2024, 9, 49013−49022

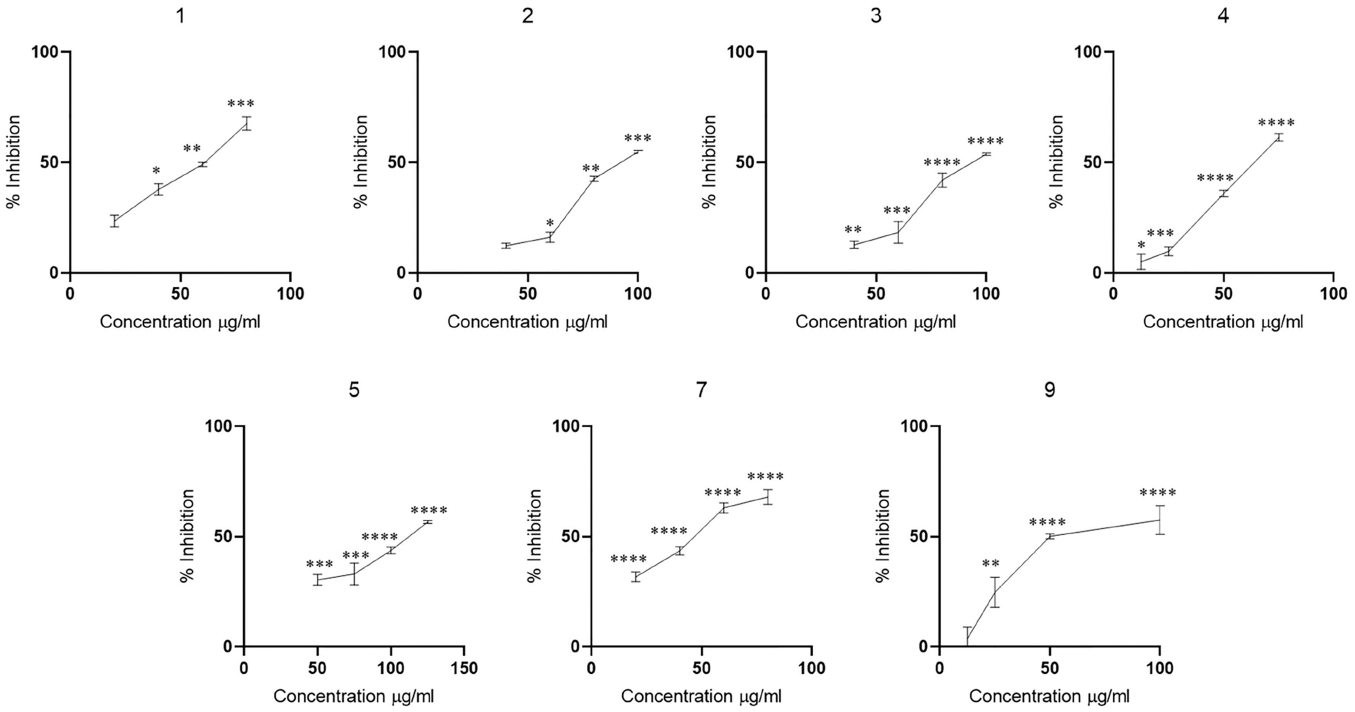

Figure 3. α-Glucosidase inhibitory activities of compounds **1**−**5**, **7**, and **9** (mean ± SD). One-way ANOVA followed by posthoc Dunnett test was performed to calculate the level of significance in comparison with respective control. *$p \leq 0.05$, **$p \leq 0.01$, ***$p \leq 0.001$, ****$p < 0.0001$.

characterized as α,β-dihydrohispidol reported earlier synthetically and *P. santalinus* heartwood appears to be only natural source.[29−31]

Compound **8** was obtained as a light yellow solid, which gave a pseudomolecular ion peak in the ESI-HR-MS spectrum at m/z 285.0750 $[M + H]^+$ (calculated for $C_{16}H_{13}O_5$, 285.0763) corresponding to molecular formula $C_{16}H_{12}O_5$ and 11 degrees of unsaturation. The yellow coloration on UV irradiation on TLC analysis, UV absorption maxima at 199, 248, and 287 nm, and IR bands corresponding to conjugated carbonyl (1609 cm^{-1}), and aromatic functionalities collectively indicated the presence of flavonoid moiety.[32,33] The ^{13}C NMR spectrum of compound **8** displayed the isoflavonoid skeleton bearing two hydroxy and one methoxy substitution, owing to the presence of a characteristic signal at δ_C/δ_H 154.80/8.12. In contrast, the ^1H NMR displayed the presence of two ABX spin systems. Based on the above-mentioned spectral data, compound **8** was characterized as calycosin or 3′-hydroxyformononetin by comparing its spectroscopic data with those reported earlier.[34]

The previously reported compounds pterostilbene (**1**),[35,36] isoliquiritigenin (**7**),[37] isopterocarpolone (**10**),[10,38] *ent*-4(15) eudesmen-1α,11-diol (**11**),[10,39] and β-eudesmol (**12**)[40,41] were also isolated and characterized by comparing their spectroscopic data with those reported in the literature.

2.2. Characterization of Artifacts. During the characterization of compound **5**, it was observed that it is getting transformed into an artifact (**5a**) in the presence of $CDCl_3$. The artifact (**5a**), purified as a white solid, displayed a pseudomolecular protonated ion peak at m/z 299.0913 $[M + H]^+$ in its ESI-MS spectrum, suggesting a loss of 14 Da ($C_{17}H_{14}O_5$). The intense fluorescence on UV irradiation on TLC analysis, UV absorption maxima at 206, 241, and 340 nm, IR bands corresponding to carbonyl (1611 cm^{-1}), aromatic functionalities in concurrence with ^1H and ^{13}C NMR spectroscopic data and its origin from compound **5** collectively indicated the presence of 2-aryl-3-carbaldehydebenzofuran skeleton.[42,43] A plausible conversion of **5** to **5a** is progressed by B ring opening with a loss of $-CH_2$ (14 Da), resulting in the generation of an aldehyde group at 6a and a hydroxyl group at 4a position supported with ^1H NMR (δ_H 10.167; $CDCl_3$; 600 MHz).

In support, it displayed two *O*-methyl carbon signals at δ_c 55.97, 55.74 and the presence of α,β-unsaturated −CHO group at δ_c 187.40. The ^1H NMR spectrum of compound **5a** displayed six aromatic signals corresponding to two sets of typical ABX patterns with the presence of two methoxy and one hydroxy substitution. A careful examination of its NMR spectroscopic data and deduced skeleton revealed a close resemblance to that of puerariafuran (2-arylbenzofuran).[42] Accordingly, artifact **5a** was characterized as melimissanol C earlier reported from *Melilotus messanensis*,[43] and its ^{13}C spectroscopic data are being reported for the first time.[43]

Considering the biosynthetic relations between pterocarpan and isoflavanone (Figure S13), and observations recorded for **5** to **5a** conversion led us to attempt the acid-catalyzed conversion of **6** to **6a**. The purified artifact (**6a**) displayed a pseudomolecular protonated ion peak at m/z 301.1075 $[M + H]^+$ in its ESI-MS spectrum corresponding to molecular formula $C_{17}H_{16}O_5$ which indicated the presence of 10 degrees of unsaturation. Its IR (3276, 1739 cm^{-1}), ^{13}C NMR {two *O*-methyl carbon signals at δ_c 55.91, 55.46, and characteristic signals at δ_c 70.09 (CH_2-2) and 45.61 (CH-3)} and ^1H NMR displaying the presence of two ABX spin systems confirmed the presence of isoflavanone skeleton. Accordingly, artifact 6a was characterized as isosativanone, and its spectroscopic data were in agreement with those reported earlier.[27]

2.3. α-Glucosidase and α-Amylase Inhibitory Activities. All the isolated compounds were evaluated for their α-glucosidase and α-amylase inhibitory activities. Among these,

https://doi.org/10.1021/acsomega.3c10180
ACS Omega 2024, 9, 49013−49022

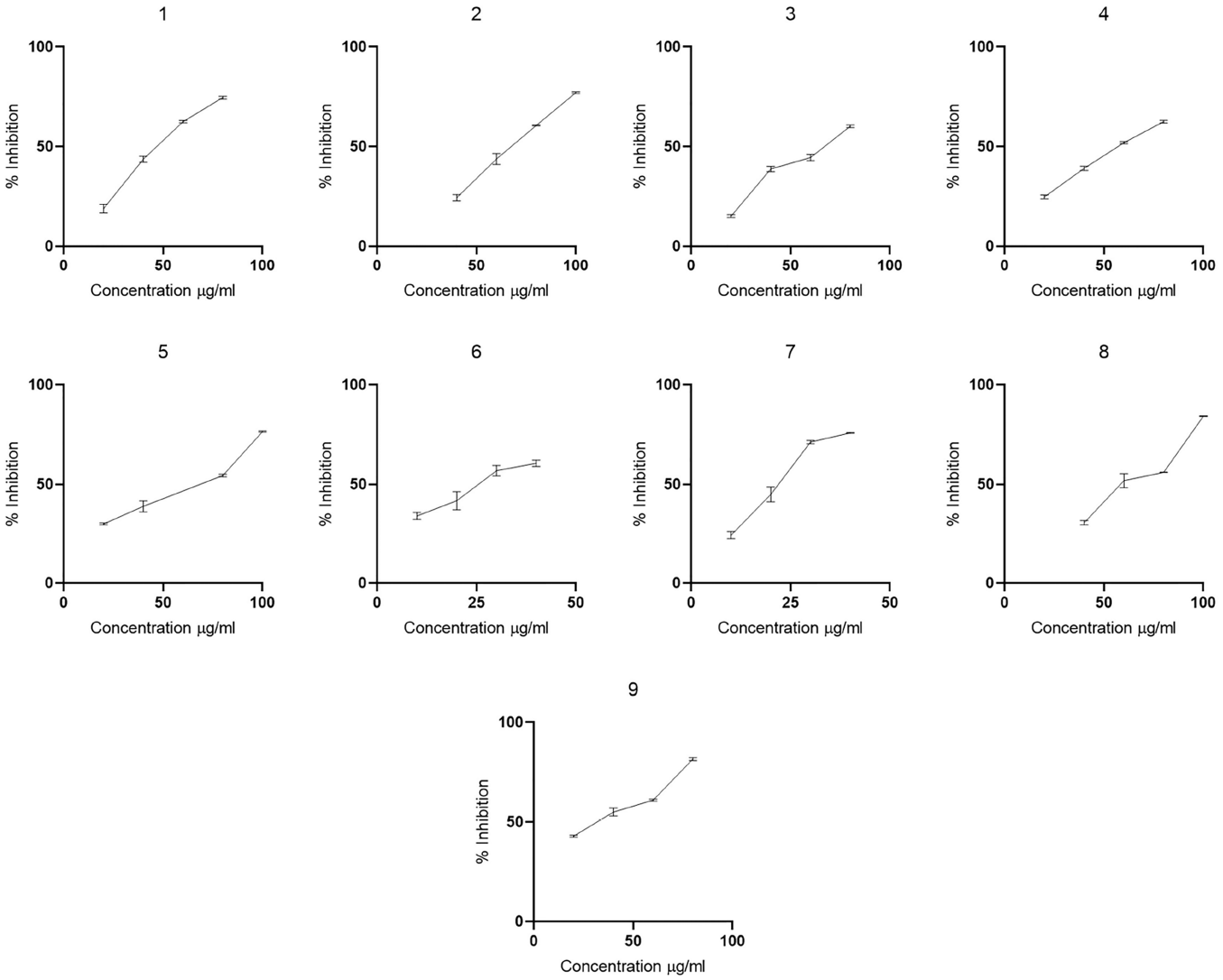

Figure 4. α-Amylase inhibitory activities of compounds **1**−**9** (mean ± SD). One-way ANOVA followed by posthoc Dunnett test was performed to calculate the level of significance in comparison with respective controls. All the data were found to be significant at $p < 0.0001$.

compounds **1**−**5**, **7**, and **9** displayed α-glucosidase inhibitory activity and demonstrated concentration-dependent inhibition (Figure 3), whereas compounds **1**−**9** also showed concentration-dependent inhibition of α-amylase (Figure 4). These compounds may be considered moderate inhibitors as compared to acarbose (IC_{50} 7.46 and 27.46 μg/mL against α-glucosidase and α-amylase, respectively).

2.4. In Silico Molecular Docking. Molecular docking was performed using Autodock to evaluate the affinity of compounds in the active site of α-glucosidase and α-amylase. Compounds were docked against α-glucosidase (source) and α-amylase (source) and compared with the standard drug (drug present in the crystal structure).

From the docking analysis, it was observed that compounds **2**−**5** and **7** showed the lowest binding energy against α-glucosidase (Table S1). Compound **2**, which shows affinity energy −9.4, established two hydrogen bonds with His279 and Arg439 via the dioxolane unit and methoxy group. Ring B, C, and D formed $\pi-\pi$ T shaped bonding with Phe157, and ring A with Phe177. A π−anion interaction of rings A and B with Asp349 was also witnessed. The methyl group formed additional $\pi-\sigma$, π−alkyl, and carbon−hydrogen bonds with Tyr71, His348, and Asp214 respectively. Similarly, compound **4** established π−anion bonding with Asp349 (C and D rings), $\pi-\pi$ T-shaped bonding to Phe157 (A and C rings), and Phe177 (D and E rings). Conventional hydrogen bonding was seen between Arg439 and dioxolane moiety. Similar binding can be witnessed in compound **3** as the molecule belongs to the same class as of compounds **2** and **4**. Interestingly, **5** did not form any hydrogen bond with the active site, but many π−alkyl and alkyl interactions were established between ring A to Ala278, Leu218, and methoxy group of ring A to Asn241, His279, and His245. Additionally, the benzofuran unit formed π−anion binding with Asp349 and a carbon-hydrogen bond with Asp214. Hydroxyl groups of compound **7** displayed conventional hydrogen bond with Asp68 and Asn241. A ring displayed π−anion interactions with Asp349 whereas B ring displayed π−alkyl interactions with Ala278 and Leu218 (Figure S14).

Compounds **2**, **3**, and **4** displayed lowest binding energy on docking with α-amylase (Table S1). Compound **2** was found to have several interactions with the binding site residues, such as the benzofuran unit of the skeleton formed $\pi-\sigma$ and π−alkyl interaction with Val163, and π−cationic and π−anionic

https://doi.org/10.1021/acsomega.3c10180
ACS Omega 2024, 9, 49013−49022

interactions were also witnessed between ring A and His201. Apart from this, an unfavorable acceptor-acceptor interaction between active site Asp197 and carbonyl unit can be seen. Compound **4** exhibits similar bindings with the enzyme where aromatic ring D interacted with His201. Another vital interaction was $\pi-\sigma$ interaction of the methoxy group with Tyr62 and the furan ring with Leu162. Furthermore, compound **3** exhibits affinity toward the active site by establishing the $\pi-\sigma$ interaction of A and D rings with Leu162 and Trp59. Several alkyl, $\pi-\sigma$ and $\pi-$alkyl interactions with Trp59, Lys200, Ile235 and His201 were displayed through methoxy groups (Figure S15).

2.5. Drug-Likeness Evaluation. The physicochemical and drug-like properties of compounds were studied using the online swissADME tool (http://www.swissadme.ch/). The bioavailability radar obtained from the swissADME indicated that most of the compounds possess drug-like characters, and compounds **4, 5, 6, 10, 11, 12**, and **6a** fall entirely within the pink radar as they possess the desired molecular weight, flexibility, saturation, and polarity (Figure S16) and displayed the desired intestinal absorption and bioavailability (Table S2).[44−47] Table S3 represents the parameters related to lipophilicity, ensuring oral bioavailability, pharmacokinetics, and pharmacodynamics. All compounds exhibited Clog *P* (calculated Log *P* < 5) in the desired range.[44,47−49] Table S4 displays the predicted water solubility using different models and most of the compounds have been identified in the moderately soluble to soluble range. Only compounds **2** and **3** are identified as poorly soluble by the Silicos-IT model.[44−47]

The gastrointestinal absorption and blood-brain permeability of the compounds were predicted with the help of the BOILED-Egg model (Table S5 and Figure S17). The SwissADME outcome for the compounds indicates that all the compounds have displayed a high gastrointestinal absorption, and except for **7**, all the compounds have been predicted to cross the blood-brain barrier. Among the screened compounds, **4, 5**, and **6** are expected to be P-gp substrates,[50] and a majority of the compounds were found to interact with one or other isoform of the enzyme except **9, 10**, and **11**. Hence, suitable drug-drug interaction studies must be considered while considering these molecules for further drug development.[50−53] It is evident from Table S6 that all the compounds have displayed negligible violations of all the five sets of rules for drug-likeness except for compound **12**, which displayed 1 violation of Muegge. They also displayed a good bioavailability score.[47] As displayed in Table S7, the compounds did not display any PAINS alerts, indicating that these molecules may not have nonspecific target binding. Still, they have displayed Brenk alerts due to the presence of stilbene, coumarin, Michael acceptor, isolated alkene, or aldehyde functionalities. They also showed one or two lead likeness violations owing to the overall physiochemical attributes.

3. CONCLUSIONS

The efforts to identify chemical constituents from the *P. santalinus* heartwood resulted in identification of one undescribed dehydropterocarpan, eleven known compounds, and two artifacts. The chemical structures of all compounds were elucidated using advanced spectroscopic techniques and it strongly advocated the presence of phenylpropanoid pathway-mediated synthesis of secondary metabolites. The genesis of artifacts and the presence of C6-C3-C6 skeleton-bearing compounds led us to predict the biosynthetic correlations (Figure S13). The in vitro bioactivity screening revealed that six compounds exhibited noteworthy inhibition of α-glucosidase, while nine compounds demonstrated active inhibition against α-amylase. It is pertinent to highlight that the identified classes of molecules have been reported to exert inhibitory action against α-glucosidase and α-amylase[54,55] and extracts derived from the *P. santalinus* bark and stem are known to inhibit the enzyme α-amylase.[56] In silico docking studies confirmed the strong affinity of isolated compounds toward both enzymes, owing to their ability to form ionic, H-bonding and hydrophobic interactions. The in silico assessment partly aligns with the in vitro assessment of the compounds wherein the compounds emerged as the moderate inhibitors of both the enzymes. Furthermore, the drug-likeness assessment illustrated that these compounds have potential characteristics that could be exploited in future research not only for the management of diabetes mellitus but also for other disease conditions.

4. MATERIALS AND METHODS

4.1. Chemical and Reagents. α-Glucosidase (*Saccharomyces cerevisiae*), α-amylase (porcine pancreas), and 4-nitrophenyl-β-D-glucopyranoside were procured from Sigma-Aldrich, India. 3,5-Dinitrosalisylic acid, acarbose, starch, sodium bicarbonate, silica gel, Celite 545, $Na_2HPO_4{\cdot}7H_2O$, and $NaH_2PO_4{\cdot}H_2O$ were procured from SRL, India. HPLC solvents were purchased from Merck, India. Milli-Q water was used for the HPLC analysis and enzyme assays.

4.2. General Experimental Methods. Plant fractions and compounds were analyzed by the analytical Shimadzu HPLC system, equipped with a Supelco Ascentis RP18, 25 cm × 4.6 mm, 5 μm column as stationary phase and mobile phases—gradient method 1 (A: water containing 0.1% formic acid and B: acetonitrile, 0−2 min 40:60 v/v; 2−22 min 5:95 v/v; 22−24 min 5:95 v/v; 24−25 min 40:60 v/v and 25−30 min 40:60 v/v for PSTF) and gradient method 2 (A: water containing 0.1% formic acid and B: acetonitrile, 0−2 min 60:40 v/v; 2−22 min 5:95 v/v; 22−24 min 5:95 v/v; 24−25 min 60:40 v/v and 25−30 min 60:40 v/v for PSEAF) at a flow rate of 1 mL/min.[57] Shimadzu SPD-M40 PDA detector was used to monitor the eluent and UV absorption profiles of compounds. Semi-preparative HPLC purification was carried out using a Waters binary HPLC system using Supelco Ascentis RP18, 25 cm × 10 mm, 5 μm (SPC-1) or Supelco Ascentis RP18, 15 cm × 10 mm, 5 μm (SPC-2) HPLC column. NMR spectra were recorded using Bruker Ultrashield 600 MHz or JEOL 400 MHz using deuterated solvents (600 μL) $CDCl_3$/MeOD. Mass spectra were recorded using Waters QToF HR-MS and IR spectra by Bruker TENSOR 27.

4.3. Plant Material. Heartwood of *Pterocarpus santalinus* L. f. was collected from the Arabari forest range, West Bengal, India, and authenticated by Central National Herbarium, Howrah (IICB/DK/008).

4.4. Extraction and Fractionation. Heartwood (4.5 kg) was coarsely powdered and subjected to maceration in methanol (72 h × 3) with occasional stirring. The extract was filtered and evaporated under reduced pressure using a rotary evaporator at 45 °C (220 g, 4.89% w/w). A portion of methanolic extract (PSME, 200 g) was suspended in 10% methanol: water and sequentially partitioned with toluene, and ethyl acetate to afford toluene fraction (PSTF, 18.1 g), and ethyl acetate fraction (PSEAF, 113.4 g).

https://doi.org/10.1021/acsomega.3c10180
ACS Omega 2024, 9, 49013−49022

4.5. Isolation and Purification. The PSTF (15 g) was eluted over a bed of silica gel with chloroform/hexane (25/75, 50/50, 75/25, and 100% v/v) to obtain four fractions (1: 8.4 g; 2: 1.01 g; 3: 0.94 g; 4: 0.42 g). Fraction 1 on silica gel column chromatography resulted in three subfractions (1A: 16 mg; 1B: 128 mg; 1C: 1.23 g) on elution with hexane−$CHCl_3$/hexane (40:60 v/v). Fraction 1C resulted in a solid precipitate (1C2; 202 mg) and supernatant (1C1; 889 mg). The 1C1 on TLC (TLC mobile phase:100% $CHCl_3$)) resulted in two spots which were then separated on prep-TLC to obtain 1C1A (79 mg) and 1C1B (49 mg); followed by semiprep HPLC purification to obtain compound **1** (ACN/H_2O, 60:40 v/v; SPC-1; rt 7.8 min; 46.5 mg) and compound **10** (ACN/H_2O, 60:40 v/v; SPC-1; rt 16.2 min; 14 mg). Subfraction 1C2 on silica gel column chromatography led to compound **11** (182.6 mg). Fraction 2 (6.85 g) on silica gel column chromatography yielded 20 subfractions (2A1−2A20). Fraction 2A7 (689 mg) on prep-TLC (1:9 v/v EtoAc: hexane) yielded compound **12** (86 mg). Fraction 2A9 (98.3 mg) on sequential crystallization and semiprep HPLC (ACN/H_2O, 60:40 v/v; SPC-2) resulted in the isolation of compounds **2** (7.7 mg; 23.5 min) and **3** (8 mg; 26.0 min).

The PSEAF (133.4 g) was fractionated over a bed of Celite 545 with hexane, chloroform, acetone, and methanol to obtain fractions P (7.7 g), Q (63.3 g), R (17.68 g), and S (10.4 g). Fractions P and Q were mixed (71 g) based on their TLC profile and further fractioned into 17 subfractions over a bed of silica gel (PQ1-PQ17). Fraction PQ5 (5.68 g) on semiprep HPLC (ACN/H_2O 60:40 v/v; SPC-1) led to the isolation of compounds **4** (4.7 mg, rt 14.9 min) and **5** (4.4 mg, rt 16.8 min). Fraction PQ8 (1.98 g) on repeated silica gel column chromatography afforded compound **6** (356 mg). Fraction R (17.68 g) on silica gel column chromatography (hexane: $CHCl_3$) yielded 12 subfractions (R1−R12). Fraction R6 (150 mg) on semipreparative HPLC purification (ACN: H_2O 50:50% v/v; SPC-1) afforded six subfractions (R6A-R6F). Fraction R6F was characterized as compound **7** (11.5 mg, rt 9.4 min), and fraction R6C on repurification (ACN: H_2O 30/70% v/v; SPC-2) led to the isolation of compound **8** (3.7 mg, rt 12.1 min). Fraction R7 (12 mg) on semipreparative HPLC purification (ACN: H_2O 30:70% v/v; SPC-1) resulted in the isolation of compound **9** (4.2 mg, rt 11.6 min).

Compound **5** generated an artifact in the presence of $CDCl_3$ in the NMR tube, which was separated on semiprep HPLC using the method 1 gradient (SPC-2) to afford compound **5** (0.9 mg; rt 7.4 min) and artifact **5a** (1.5 mg; rt 14.2 min).

4.6. Acid Treatment of Variabilin (6). Compound **6** was treated with 4N HCl in methanol under reflux for 12 h. The reaction mixture was neutralized with NaOH and partitioned with ethyl acetate. A yellow-colored ethyl acetate layer was collected and dried under a rotary evaporator. It was further purified using a semiprep HPLC (ACN: H_2O 1:1 v/v; rt 11.01 min) to obtain compound **6a**.

4.7. α-Glucosidase Inhibitory Assay. In vitro α-glucosidase inhibitory assay was performed by mixing 25 μL of 0.5 U enzyme (0.1 M phosphate buffer; pH 6.8) and 25 μL of samples and incubated for 15 min at 37 °C in a 96-well-plate. After incubation, 25 μL of substrate (0.5 mM; 0.1 M phosphate buffer; pH 6.8) was added and incubated for 30 min at 37 °C. In the end, 100 μL of 0.2 M Na_2CO_3 solution was added, and the resultant color was measured at 405 nm (Thermo Scientific Multiskan FC). The uninhibited enzyme was taken as control, and acarbose was used as the reference standard. An appropriate DMSO blank was used, and the final concentration of DMSO was maintained below 5%. The assay was performed in triplicate.[58,59]

4.8. α-Amylase Inhibitory Activity. 200 μL of α-amylase (1 U/ml; 20 mM phosphate buffer; pH 6.8) was incubated with 100 μL of sample for 10 min at 25 °C. After incubation, 200 μL of starch solution (1% w/v) was added and again incubated at 25 °C for 10 min. The reaction was terminated by the addition of 200 μL of DNS reagent (96 mM dinitro salicylic acid). The resultant reaction mixture was heated at 80−90 °C for 20 min, and absorbance was measured at 540 nm (Thermo Scientific Multiskan FC). The uninhibited enzyme was taken as control, and acarbose was used as the reference standard. An appropriate DMSO blank was used, and the final concentration of DMSO was maintained below 5%. The assay was performed in triplicate.[58,59]

4.9. In Silico Molecular Docking Studies. Molecular docking studies were employed with α-glucosidase and α-amylase to predict the binding modes of the isolated compounds. The crystal form of pig-pancreatic α-amylase (PDB: 3L2M) was downloaded from the RCSB PDB archive, and the structure was refined by eliminating water atoms. As the 3D structure of *Saccharomyces cerevisiae* α-(1,4)-glucosidase is not available, we followed the homology modeling for the *S. cerevisiae* α-(1,4)-glucosidase reported earlier.[60] Docking studies were carried out on the Autodock Vina 1.1.2[61] program using the Lamarckian Genetic Algorithm and Empirical Binding Free Energy scoring function.[62] The structures of compounds were saved in PDB format in their minimized energy form. This was followed by importing ligand molecules in Autodock Vina software, and after hydrogen addition, files were saved in PDBQT format. Similarly, both target proteins were also saved in the PDBQT format. For α-amylase, the sizes of the grid box (*xyz* points) were set as 22, 22, and 20, while the grid centers were designated at dimensions (*x*, *y*, and *z*) 35.067, 35.613 and 52.211 with the spacing of 1.0 Å. Similarly, for α-glucosidase, the sizes of the grid box (*xyz* points) were set as 22, 24, and 22, while the grid centers were designated at dimensions (*x*, *y*, and *z*) 19.614, −6.998 and 21.051 with the spacing of 1.0 Å. The docked output files were analyzed for the best score values, and interactions between the ligands and the enzyme binding site were observed using a visualization tool like Discovery Studio Visualizer. v21.1.0.20298.

4.10. In Silico ADME Prediction. In vitro studies of most compounds isolated from the *P. santalinus* heartwood showed considerable α-glucosidase and α-amylase inhibitory activity and could also be responsible for the other therapeutic potential.[1] Therefore, to access their drug-like-ness properties, we utilized the SwissADME web tool.[47] The molecular structure of isolated compounds was introduced in the simplified molecular-input line-entry specification (SMILES) for computational simulation, and the predicted physicochemical properties were studied (http://www.swissadme.ch/).

■ ASSOCIATED CONTENT

Supporting Information

The Supporting Information is available free of charge at https://pubs.acs.org/doi/10.1021/acsomega.3c10180.

Spectroscopic data of compound **5** and data associated with in silico and SwissADME analysis (PDF)

https://doi.org/10.1021/acsomega.3c10180
ACS Omega 2024, 9, 49013−49022

AUTHOR INFORMATION

Corresponding Author

Deepak Kumar − *Organic and Medicinal Chemistry Division, CSIR-Indian Institute of Chemical Biology (IICB), Kolkata 700032, India;* orcid.org/0000-0002-8292-1684; Phone: +91-33-24995804; Email: deepak@iicb.res.in, dkseervi@gmail.com

Authors

Priya Darshani − *Organic and Medicinal Chemistry Division, CSIR-Indian Institute of Chemical Biology (IICB), Kolkata 700032, India; National Institute of Pharmaceutical Education and Research (NIPER), Kolkata 700054, India*

Shreya Sen Sarma − *Organic and Medicinal Chemistry Division, CSIR-Indian Institute of Chemical Biology (IICB), Kolkata 700032, India*

Rahul L. Gajbhiye − *National Institute of Pharmaceutical Education and Research (NIPER), Hajipur 844102, India*

Amit K. Srivastava − *Cancer Biology & Inflammatory Disorder Division, CSIR-Indian Institute of Chemical Biology (IICB), Kolkata 700032, India;* orcid.org/0000-0002-4941-0591

Complete contact information is available at: https://pubs.acs.org/10.1021/acsomega.3c10180

Author Contributions

P.D.: investigation, data analysis, bioactivity, data curation, writing original draft; S.S.S.: investigation, data analysis, data curation, writing original draft; R.L.G.: docking studies, A.K.S.: valuable suggestion; D.K.: project administration, conceptualization, supervision, writing and revision of the manuscript; D.K., A.K.S.: funding acquisition. P.D. and S.S.S. equally contributed to this work.

Notes

The authors declare no competing financial interest.

ACKNOWLEDGMENTS

D.K. and A.K.S. are thankful to the National Biodiversity Authority (NBA), Chennai, India, for the financial support (Tech/Gen1/22/149/17/18-19/4294 and 4292). Financial support from HCP-40, MLP-138, and in-house funding (P07/P50) are also acknowledged. P.D. and S.S.S. received fellowships from NIPER-Kolkata and NBA, respectively. Instrumentation support from the CIF CSIR-IICB is highly acknowledged. The data and results presented in this article are part of Ph.D. thesis of PD.

REFERENCES

(1) Dahat, Y; Saha, P; Mathew, J. T.; Chaudhary, S. K.; Srivastava, A. K.; Kumar, D Traditional uses, phytochemistry and pharmacological attributes of *Pterocarpus santalinus* and future directions: A review. *J Ethnopharmacol* **2021**, *276*, No. 114127.

(2) Teixeira da Silva, J. A.; Kher, M. M.; Soner, D; Nataraj, M Red sandalwood (*Pterocarpus santalinus* L. f.): biology, importance, propagation and micropropagation. *J For Res* **2019**, *30*, 745−754.

(3) Arunakumara, K. K. I. U.; Walpola, B. C.; Subasinghe, S.; Yoon, M. H. *Pterocarpus santalinus* linn. f. (Rath handun): A review of its botany, uses, phytochemistry and pharmacology. *J. Korean Soc. Appl. Biol. Chem.* **2011**, *54*, 495−500.

(4) Wu, S. F.; Chang, F. R.; Wang, S. Y.; Hwang, T. L.; Lee, C. L.; Chen, S. L.; et al. Anti-inflammatory and cytotoxic neoflavonoids and benzofurans from *Pterocarpus santalinus*. *J Nat Prod* **2011**, *74*, 989−996.

(5) Wasilewicz, A.; Zwirchmayr, J.; Kirchweger, B.; Bojkova, D.; Cinatl, J.; Rabenau, H. F.; et al. Discovery of anti-SARS-CoV-2 secondary metabolites from the heartwood of *Pterocarpus santalinus* using multi-informative molecular networking. *Front. Mol. Biosci.* **2023**, *10*, No. 1202394.

(6) Ghali, E. N. H. K.; Maurya, D. K.; Meriga, B. Radioprotective properties of *Pterocarpus santalinus* chloroform extract in murine splenic lymphocytes and possible mechanism. *Cancer Biother. Radiopharm.* **2018**, *33*, 427−437.

(7) Mazzio, E; Deiab, S; Park, K; Soliman, K. F. A. High throughput screening to identify natural human monoamine oxidase B inhibitors. *Phyther Res* **2013**, *27*, 818−828.

(8) Kameswara Rao, B; Giri, R; Kesavulu, M. M.; Apparao, C Effect of oral administration of bark extracts of *Pterocarpus santalinus* L. on blood glucose level in experimental animals. *J Ethnopharmacol* **2001**, *74*, 69−74.

(9) Cho, J. Y.; Park, J; Kim, P. S.; Yoo, E. S.; Baik, K. U.; Park, M. H. Savinin, a lignan from *pterocarpus santalinus* inhibits tunror necrosis factor-α production and T cell proliferation. *Biol. Pharm. Bull.* **2001**, *24*, 167−171.

(10) Li, L; Tao, R. H.; Wu, J. M.; Guo, Y. P.; Huang, C; Liang, H. G.; et al. Three new sesquiterpenes from *Pterocarpus santalinus*. *J Asian Nat Prod Res* **2018**, *20*, 306−312.

(11) Arnone, A; Camarda, L; Merlini, L; Nasini, G Structures of the red sandalwood pigments santalins A and B. *J. Chem. Soc., Perkin Trans.* **1975**, *1*, 186−194.

(12) Zwirchmayr, J; Schachner, D; Grienke, U; Rudžionytė, I; de Martin, R; Dirsch, V. M.; et al. Biochemometry identifies suppressors of pro-inflammatory gene expression in *Pterocarpus santalinus* heartwood. *Phytochemistry* **2023**, *212*, No. 113709.

(13) El-badawy, R. E.; Ibrahim, K. A.; Hassan, N. S.; El-sayed, W. M. *Pterocarpus santalinus* ameliorates streptozotocin-induced diabetes mellitus via anti-inflammatory pathways and enhancement of insulin function. *Iran. J. Basic Med. Sci.* **2018**, *22*, 932−939.

(14) Kumar, D; Ghosh, R; Pal, B. C. α-Glucosidase inhibitory terpenoids from *Potentilla fulgens* and their quantitative estimation by validated HPLC method. *J Funct Foods* **2013**, *5*, 1135−1141.

(15) Yin, Z; Zhang, W; Feng, F; Zhang, Y; Kang, W α-Glucosidase inhibitors isolated from medicinal plants. *Food Sci Hum Wellness* **2014**, *3*, 136−174.

(16) Shibano, M; Henmi, A; Matsumoto, Y; Kusano, G; Miyase, T; Hatakeyama, Y Studies on the index compounds for HPLC analysis of *Glycyrrhiza uralensis*. *Heterocycles* **1997**, *45*, 2053−2060.

(17) Yenesew, A.; Derese, S.; Irungu, B.; Midiwo, J. O.; Waters, N. C.; Liyala, P.; et al. Flavonoids and isoflavonoids with antiplasmodial activities from the root bark of *Erythrina abyssinica*. *Planta Med.* **2003**, *69*, 658−661.

(18) Njamen, D; Talla, E; Mbafor, J. T.; Fomum, Z. T.; Kamanyi, A; Mbanya, J. C.; et al. Anti-inflammatory activity of erycristagallin, a pterocarpene from *Erythrina mildbraedii*. *Eur. J. Pharmacol.* **2003**, *468*, 67−74.

(19) Fowler, K. J.; Ellis, J. L.; Morrow, G. W. 6-Endo Heck cyclization of 3-(2-Iodophenoxy)methylbenzofurans: A useful approach to pterocarpenes. *Synth. Commun.* **2013**, *43*, 1676−1682.

(20) Farkas, L; Gottsegen, À; Nóagrádi, M; Antus, S Synthesis of sophorol, violanone, lonchocarpan, claussequinone, philenopteran, leiocalycin, and some other natural isoflavonoids by the oxidative rearrangement of chalcones with thallium(III) nitrate. *J. Chem. Soc., Perkin Trans.* **1974**, *1*, 305−312.

(21) Adityachaudhury, N; Gupta, P. K. A new pterocarpan and coumestan in the roots of *Flemingia chappar*. *Phytochemistry* **1973**, *12*, 425−428.

(22) Chen, Y; Wei, X; Xie, H; Deng, H Antioxidant 2-phenylbenzofurans and a coumestan from *Lespedeza virgata*. *J Nat Prod* **2008**, *71*, 929−932.

(23) Ferreira, D; Kamara, B. I.; Brandt, E. V.; Joubert, E Phenolic compounds from *Cyclopia intermedia* (Honeybush Tea). 1. *J. Agric. Food Chem.* **1998**, *46*, 3406−3410.

https://doi.org/10.1021/acsomega.3c10180
ACS Omega 2024, 9, 49013−49022

(24) Mackey, K; Pardo, L. M.; Prendergast, A. M.; Nolan, M. T.; Bateman, L. M.; McGlacken, G. P. Cyclization of 4-phenoxy-2-coumarins and 2-pyrones via a double C-H activation. *Org. Lett.* **2016**, *18*, 2540−2543.
(25) Nayak, M; Jung, Y; Kim, I Syntheses of pterocarpenes and coumestans via regioselective cyclodehydration. *Org Biomol Chem* **2016**, *14*, 8074−8087.
(26) Tang, L; Pang, Y; Yan, Q; Shi, L; Huang, J; Du, Y; et al. Synthesis of coumestan derivatives via $FeCl_3$-mediated oxidative ring closure of 4-hydroxy coumarins. *J. Org. Chem.* **2011**, *76*, 2744−2752.
(27) Ciesielski, P; Metz, P Asymmetric one-pot transformation of isoflavones to pterocarpans and its application in phytoalexin synthesis. *Nat Commun* **2020**, *11*, 1−8.
(28) Kurosawa, K; Ollis, W. D.; Sutherland, I. O.; Gottlieb, O. R. Variabilin, a 6a-hydroxypterocarpan from *Dalbergia variabilis*. *Phytochemistry* **1978**, *17*, 1417−1478.
(29) Breytenbach, J. C.; Rall, G. J. H.; Roux, D. G.; Hull, W. E. Neoraufuracin and ambofuracin. Two novel 2-benzyl-2-O-(methyl-*β*-D-glucopyranos-2-yl)-trans-2,3-dihydrobenzofurans. Synthesis of the methylated aglycone. *J Chem Soc Perkin Trans 1* **1982**, 1157−1162.
(30) Huang, L; Wall, M. E.; Wani, M. C.; Navarro, H; Santisuk, T; Reutrakul, V; et al. New compounds with DNA strand-scission activity from the combined leaf and stem of *Uvaria hamiltonii*. *J Nat Prod* **1998**, *61*, 446−450.
(31) Venkateswarlu, S; Murty, G. N.; Satyanarayana, M; Siddaiah, V Design, synthesis and biological activities of dihydroaurones. *Asian J. Chem.* **2021**, *33*, 1396−1402.
(32) Jung, K; Jeon, J. S.; Ahn, M. J.; Kim, C. Y.; Kim, J Preparative isolation and purification of flavonoids from *Pterocarpus saltalinus* using centrifugal partition chromatography. *J Liq Chromatogr Relat Technol* **2012**, *35*, 2462−2470.
(33) Krysa, M; Szymańska-Chargot, M; Zdunek, A FT-IR and FT-Raman fingerprints of flavonoids − A review. *Food Chem.* **2022**, *393*, No. 133430.
(34) Kobayashi, M; Noguchi, H; Sankawa, U Formation of chalcones and isoflavones by callus culture of *Glycyrrhiza uralensis* with different production patterns. *Chem Pharm Bull* **1985**, *33*, 3811−3816.
(35) Pettit, G. R.; Singh, S. B.; Schmidt, J. M.; Niven, M. L.; Hamel, E.; Lin, C. M. Isolation, structure, synthesis, and antimitotic properties of combretastatins b-3 and b-4 from *Nombretum caffrum*. *J. Nat. Prod.* **1988**, *51*, 517−527.
(36) Rimando, A. M.; Pezzuto, J. M.; Farnsworth, N. R.; Santisuk, T; Reutrakul, V Revision of the NMR assignments of pterostlbene and of dihydrodehydrodiconiferyl alcohol: Cytotoxic constituents from *Anogeissus acuminata*. *Nat Prod Lett* **1994**, *4*, 267−272.
(37) Lee, E. J.; Shaikh, S.; Ahmad, K.; Ahmad, S. S.; Lim, J. H.; Park, S.; et al. Isolation and characterization of compounds from *Glycyrrhiza uralensis* as therapeutic agents for the muscle disorders. *Int. J. Mol. Sci.* **2021**, *22*, 876.
(38) Shaaban, K. A.; Singh, S.; Elshahawi, S. I.; Wang, X.; Ponomareva, L. V.; Sunkara, M.; et al. The native production of the sesquiterpene isopterocarpolone by Streptomyces sp. RM-14-6. *Nat. Prod. Res.* **2014**, *28*, 337−339.
(39) Isaka, M; Palasarn, S; Lapanun, S; Chanthaket, R; Boonyuen, N; Lumyong, S *γ*-lactones and ent-eudesmane sesquiterpenes from the endophytic fungus Eutypella sp. BCC 13199. *J Nat Prod* **2009**, *72*, 1720−1722.
(40) Lim, C. K.; Hemaroopini, S.; Say, Y. H.; Jong, V. Y. M. Cytotoxic compounds from the stem bark of *Calophyllum soulattri*. *Nat. Prod. Commun.* **2017**, *12*, 1469−1471.
(41) Kumar, N; Ravindranath, B; Seshadri, T. R. Terpenoids of *Pterocarpus santalinus* heartwood. *Phytochemistry* **1974**, *13*, 633−636.
(42) Jang, D. S.; Kim, J. M.; Lee, Y. M.; Kim, Y. S.; Kim, J. H.; Kim, J. S. Puerariafuran, a new inhibitor of advanced glycation end products (AGEs) isolated from the roots of *Pueraria lobata*. *Chem Pharm Bull* **2006**, *54*, 1315−1317.
(43) Macías, F. A.; Simonet, A. M.; Galindo, J. C.; Castellano, D. Bioactive phenolics and polar compounds from *Melilotus messanensis*. *Phytochemistry* **1999**, *50*, 35−46.
(44) Veber, D. F.; Johnson, S. R.; Cheng, H. Y.; Smith, B. R.; Ward, K. W.; Kopple, K. D. Molecular properties that influence the oral bioavailability of drug candidates. *J. Med. Chem.* **2002**, *45*, 2615−2623.
(45) Banik, I; Roy, M. N. Study of solute−solvent interaction of some bio-active solutes prevailing in aqueous ascorbic acid solution. *J. Mol. Liq.* **2012**, *169*, 8−14.
(46) 2021 71 Ibrahim, Z. Y.; Uzairu, A; Shallangwa, G. A.; Abechi, S. E. Pharmacokinetic predictions and docking studies of substituted aryl amine-based triazolopyrimidine designed inhibitors of Plasmodium falciparum dihydroorotate dehydrogenase (PfDHODH). Futur. *J. Pharm. Sci.* **2021**, *7*, 1−10.
(47) 2017 71 Daina, A; Michielin, O; Zoete, V Swiss ADME: a free web tool to evaluate pharmacokinetics, drug-likeness and medicinal chemistry friendliness of small molecules. *Sci Reports* **2017**, *7*, 1−13.
(48) Arnott, J. A.; Planey, S. L. The influence of lipophilicity in drug discovery and design. *Expert Opin Drug Discov* **2012**, *7*, 863−875.
(49) Benet, L. Z.; Hosey, C. M.; Ursu, O; Oprea, T. I. BDDCS, the Rule of 5 and drugability. *Adv Drug Deliv Rev* **2016**, *101*, 89−98.
(50) Finch, A; Pillans, P P-glycoprotein and its role in drug-drug interactions. *Aust Prescr* **2014**, *37*, 137−139.
(51) Kondža, M; Bojić, M; Tomić, I; Maleš, Ž; Rezić, V; Ćavar, I Characterization of the CYP3A4 enzyme inhibition potential of selected flavonoids. *Molecules* **2021**, *26*, 3018.
(52) Ogu, C. C.; Maxa, J. L. Drug interactions due to cytochrome P450. *Baylor Univ Med Cent Proc* **2000**, *13*, 421−423.
(53) Esteves, F; Rueff, J; Kranendonk, M The central role of cytochrome P450 in xenobiotic metabolism—a brief review on a fascinating enzyme family. *J Xenobiotics* **2021**, *11*, 94−114.
(54) Dendup, T; Prachyawarakorn, V; Pansanit, A; Mahidol, C; Ruchirawat, S; Kittakoop, P *α*-Glucosidase inhibitory activities of isoflavanones, isoflavones, and pterocarpans from *Mucuna pruriens*. *Planta Med* **2014**, *80*, 604−608.
(55) Dirir, A. M.; Daou, M; Yousef, A. F.; et al. A review of alpha-glucosidase inhibitors from plants as potential candidates for the treatment of type-2 diabetes. *Phytochem Rev* **2022**, *21*, 1049−1079.
(56) Pandey, B. P.; Prakash Pradhan, S; Joshi, P; Adhikari, K Antioxidant and enzymes inhibitory activities of leaf extracts of plant species traditionally used for medicinal and spiritual purposes in Nepal. *J Herbs Spices Med Plants* **2022**, *28*, 265−280.
(57) Darshani, P; Sen Sarma, S; Tripathy, P; Kumar, D Ultrasonication-assisted optimization of pterostilbene extraction from *Pterocarpus santalinus* heartwood using response surface methodology. *Ind Crops Prod* **2024**, *213*, No. 118409.
(58) Kumar, D; Gupta, N; Ghosh, R; Gaonkar, R. H.; Pal, B. C. *α*-Glucosidase and *α*-amylase inhibitory constituent of *Carex baccans*: Bio-assay guided isolation and quantification by validated RP-HPLC−DAD. *J Funct Foods* **2013**, *5*, 211−218.
(59) Kumar, D; Shah, V; Ghosh, R; Pal, B. C. A new triterpenoid saponin from *Glinus oppositifolius* with *α*-glucosidase inhibitory activity. *J Funct Foods* **2013**, *27*, 624−630.
(60) Gupta, S. J.; Dutta, S; Gajbhiye, R. L.; Jaisankar, P; Sen, A. K. Synthesis, in vitro evaluation and molecular docking studies of novel amide linked triazolyl glycoconjugates as new inhibitors of *α*-glucosidase. *Bioorg Chem* **2017**, *72*, 11−20.
(61) Trott, O; Olson, A. J. Auto Dock Vina: Improving the speed and accuracy of docking with a new scoring function, efficient optimization, and multithreading. *J. Comput. Chem.* **2010**, *31*, 455−461.
(62) Morris, G. M.; Goodsell, D. S.; Halliday, R. S.; Huey, R; Hart, W. E.; Belew, R. K.; et al. Automated docking using a lamarckian genetic algorithm and an empirical binding free energy function. *J. Comput. Chem.* **1998**, *19*, 1639−1662.

https://doi.org/10.1021/acsomega.3c10180
ACS Omega 2024, 9, 49013−49022